Soft Matter

RSC Publishing

PAPER

View Article Online
View Journal

Cite this: DOI: 10.1039/c3sm52336e

Self-assembly of PBzMA-*b*-PDMAEMA diblock copolymer films at the air–water interface and deposition on solid substrates *via* Langmuir–Blodgett transfer

P. Cecilia dos Santos Claro,[ad] Marcos E. Coustet,[a] Carolina Diaz,[abd] Eliana Maza,[a] M. Susana Cortizo,[ad] Félix G. Requejo,[ad] Lía I. Pietrasanta,[bcd] Marcelo Ceolín[ad] and Omar Azzaroni*[ad]

The aggregation behavior and morphological characteristics of amphiphilic block copolymer polybenzyl methacrylate-*block*-poly(dimethylamino)ethyl methacrylate (PBzMA-*b*-PDMAEMA) at the air–water interface were investigated through surface pressure measurements, atomic force microscopy (AFM) imaging, electrochemical measurements and X-ray reflectivity. Ionization of PDMAEMA blocks significantly affects the isotherms of the surface films at the air–water interface and, consequently, originates different morphologies of Langmuir–Blodgett films obtained under different experimental conditions. At low pH the PDMAEMA blocks are fully protonated and therefore dissolved in the aqueous subphase. Under this condition, the effects of the solubility and electrostatic repulsion of submerged PDMAEMA chains prevail over hydrophobic interactions and the Langmuir film exhibits low surface pressure at large molecular area values. Upon compression, the isotherm shows a pseudoplateau corresponding to the "*pancake-to-brush*" transition followed by an increase in surface pressure at smaller MMA values. These results were correlated with the morphological features of Langmuir–Blodgett films transferred onto silicon substrates, where dispersed dot-like domains that gradually transformed into an island-like structure, followed by further percolation into a continent-like morphology, were observed through AFM imaging. On the other hand, at high pH the isotherm is more expanded and the film exhibits higher surface pressure at relatively high MMA values due to the strong repulsive interactions between interface-confined hydrophobic aggregates constituted of PBzMA cores and neutral PDMAEMA shells. In this case, the AFM results show a structural evolution from circular and quasi-hexagonally packed micelles, followed by a worm-like structure that collapses into a homogeneous film. Furthermore, the study of the copolymer behavior under different subphase ionic strength conditions confirmed the critical role of electrostatic interactions in determining the characteristics of the isotherm. We could also demonstrate that our system follows accurately the scaling relationship for surface pressure of annealed brushes. Complementary studies performed by means of X-ray reflectivity were carried out to probe the buried interfacial structure of the diblock copolymer film, corroborating that the organization of both blocks on the silicon substrates is strongly dependent on the pH conditions of the subphase during the LB transfer.

Received 4th September 2013
Accepted 22nd September 2013

DOI: 10.1039/c3sm52336e

www.rsc.org/softmatter

Introduction

The design and preparation of polymer films based on self-assembled diblock copolymers[1,2] has garnered much attention from researchers in recent years owing to the myriad of applications that rely on the use of nanostructured soft interfaces, namely, active films for biosensors, devices for optoelectronics or templates for nanopatterning, among other examples.[3–6]

Within this framework, research efforts on Langmuir–Blodgett (LB) films consisting of monolayers of polymers are rapidly expanding.[7] The renewed interest, which has been

[a]*Instituto de Investigaciones Fisicoquímicas Teóricas y Aplicadas (INIFTA), Departamento de Química, Facultad de Ciencias Exactas, Universidad Nacional de La Plata (UNLP), CONICET, La Plata, Argentina. E-mail: azzaroni@inifta.unlp.edu.ar; Web: http://softmatter.quimica.unlp.edu.ar*

[b]*Centro de Microscopías Avanzadas (CMA), Facultad de Ciencias Exactas y Naturales, Universidad de Buenos Aires, Ciudad Autónoma de Buenos Aires, Argentina*

[c]*Departamento de Física, Facultad de Ciencias Exactas y Naturales, Universidad de Buenos Aires, Ciudad Autónoma de Buenos Aires, Argentina*

[d]*Consejo Nacional de Investigaciones Científicas y Técnicas (CONICET), C1033AAJ, Buenos Aires, Argentina*

manifested in the use of the LB technique to prepare thin polymer films, stems from the tight control over the molecular aggregation state of the macromolecular material at the air–water interface.[8,9] In this particular case surface pressure plays a key role as an external parameter with the ability to trigger aggregation and self-organization processes in the monolayer.[10] Compared with LB films of homopolymers and random copolymers, the formation of surface monolayers of amphiphilic block copolymers has been studied to a much lesser extent. Due to their intrinsic ability to self-assemble into a variety of self-organized structures, amphiphilic block copolymers represent key enabling building blocks for the formation of nanostructured soft interfaces displaying different morphologies.[11–15]

However, the spontaneous formation of nanostructured films *via* self-assembly pathways requires detailed knowledge and control of these nanoarchitectures from the very early stages of self-organization. Indeed, the formation of morphologically defined ultrathin block copolymer films strongly demands an in-depth understanding of the processes taking place during surface area compression at the air–water interface. This, in turn, is essential to govern the factors that control them. In most of the cases amphiphilic diblock copolymers self-assemble at the air–water interface forming "surface micelles". In a typical scenario the hydrophobic blocks aggregate to form self-segregated isolated structures stabilized by the hydrophilic counterparts spread on the water surface, *i.e.* the corona. As the film is compressed, these nanobuilding blocks confined at the air–water interface suffer from a variety of structural reorganizations that concomitantly lead to different morphological transitions. These systems exhibit a trend of increasing morphological complexity when the subphase pH controls the ionization of the hydrophilic block and, hence, the solubility of the corona chain of the surface micelles. For charged amphiphiles, a significant contribution to surface pressure from the electrostatic term needs to be considered, independently from van der Waals interactions. In some cases these macromolecular systems have been referred to as "polymer brushes at the air–water interface".[16]

The role of subphase pH in the aggregation of amphiphilic block copolymers displaying ionizable hydrophilic blocks has been intensively studied in a wide variety of systems. For example, the solubility of neutral vinylpyridine blocks in polystyrene-*b*-poly(vinylpyridine) (PS-*b*-PVP) copolymers is strongly dependent on pH. The influence of subphase pH has been exploited by Chung *et al.* to control the degree of desorption of the blocks into the water subphase in order to create different surface morphologies at the air–water interface.[17] Similarly Langmuir films of diblock copolymers constituted of polystyrene as the hydrophobic segment and poly(acrylic acid) as the hydrophilic counterpart (PS-*b*-PAA) exhibit a broad variety of morphological transitions that lead to films with different nanoscale features.[18–21] The responsiveness of PAA to subphase pH changes leads to the expansion of the ionized blocks in the aqueous phase at high pH, and contraction to a more globular form at low pH.[22] Extensive systematic studies from different research groups reflect that the morphological richness of diblock copolymers assembled *via* Langmuir–Blodgett techniques is heavily reliant on the chemical identities of the constituting building blocks. Hence, the investigation of unexplored pH-responsive diblock copolymer systems would open doors to new nanostructure forming materials as well as offer interesting opportunities to design responsive interfacial architectures.

To our knowledge, this is the first report on the self-assembly and aggregation of polybenzyl methacrylate-*block*-poly(2-(dimethylamino)ethyl methacrylate) copolymer films at the air–water interface followed by the deposition on solid substrates using the Langmuir–Blodgett technique. In this work, we investigated the effect of subphase pH and ionic strength on the surface micellization behavior of poly(benzyl methacrylate)-*block*-poly(2-(dimethylamino)ethyl methacrylate) at the air–water interface and correlated the observed physicochemical behaviour with the surface morphologies of Langmuir–Blodgett films obtained under different experimental conditions.

Experimental section

Chemicals and reagents

Benzyl methacrylate (BzMA, 96%), 2-(dimethylamino)ethyl methacrylate (DMAEMA, 98%) monomers, the initiator, 1-methoxy-1-trimethylsiloxy-2-methyl propene (MTS), tetrabutylammonium hydroxide and benzoic acid were all purchased from Aldrich, Argentina. The monomers were purified by vacuum distillation and kept on an activated 4A molecular sieve until use. Chloroform (Carlo Erba, 99%) for HPLC was used as purchased. Tetrahydrofuran (THF, Carlo Erba, 99.8%), the polymerization solvent, was refluxed under nitrogen over sodium (Na)/benzophenone (BP) in a controlled atmosphere still until blue color of medium. The THF was then distilled into a flask with the activated 4A molecular sieve and stopped with a septum stopcock. The polymerization catalyst, tetrabutylammonium bibenzoate (TBABB), was prepared from the reaction of tetrabutylammonium hydroxide with benzoic acid according to Dicker *et al.*[23] and was kept under vacuum until use.

Block copolymer synthesis and characterization

The diblock copolymer comprising benzyl methacrylate (BzMA) and 2-(dimethylamino)ethyl methacrylate (DMAEMA) units was prepared by group transfer polymerization[24,25] (GTP) in THF using a glass reactor under dry nitrogen and standard Schlenk techniques as described elsewhere.[26] The presence and nature of the different groups were determined by ^{1}HNMR. The ^{1}H-NMR spectrum of the copolymer was recorded with a Varian-200 MHz (Mercury 200) at 35 °C in $CDCl_3$. Tetramethylsilane (TMS) was used as an internal standard. δ (ppm): 1.06–0.73 (–CH_3, m, 6H); 1.91–1.79 (–CH_2–, m, 4H); 2.28 (–N(CH_3)$_2$, s, 6H); 2.56 (–CH_2–N<, t, 2H); 4.06 (–O–CH_2–, t, 2H); 4.90 (Ar–CH_2–, s, 2H); 7.28 (Ar*H*, m, 5H). The molecular weight distribution and the average molecular weights were determined by size exclusion chromatography (SEC), using a LKB-2249 instrument at 25 °C. A series of four μ-Styragel® columns, ranging in pore size 10^5, 10^4, 10^3, 100 Å, was used with chloroform as an eluent.

The sample concentration was 4–5 mg ml^{-1} and the flow rate was 0.5 ml min^{-1}. The polymer was detected using a Shimadzu (SPD-10A) UV/VIS detector at 254 nm. The calibration was done with polystyrene standards supplied by Polymer Laboratories and Polysciences, Inc. The resulting number-average molecular weight (M_n) is 2.6 kD and 4.5 kDa for the first block (homopolymer) and the final copolymer respectively. A dispersity ($D = M_w/M_n$ where M_w is the weight-average molecular weight) of 1.2 for both, homo and block copolymers was determined by SEC, which agrees with the expected values for this type of polymerization.[26] The copolymer composition (56 : 44) was estimated from the integral ratio of the peaks of aromatic and methylene hydrogen at 7.28 and 4.06 ppm, respectively, from the ^{1}H-NMR spectrum.

Langmuir–Blodgett technique

Surface pressure measurements were performed using a Langmuir–Blodgett trough (KSV 5000, total area = 852 cm^2) at a symmetric compression rate of 10 mm min^{-1}. Langmuir films of PBzMA-*b*-PDMAEMA were formed at the air–water interface by spreading, unless otherwise indicated, 30 μl of polymer solution in chloroform (3.4 mg ml^{-1}) using a Hamilton microliter syringe, on the MilliQ water subphase. The temperature was kept constant at 24 °C ± 1 °C, using a circulating water bath (Julabo, F12MC). The pH of the subphase was adjusted prior to spreading of the copolymer solution, with HCl or NaOH and the ionic strength was kept constant with KCl. Langmuir films were transferred onto silicon wafers treated with $NH_4OH : H_2O_2 : H_2O$ (1 : 1 : 5), keeping the surface pressure constant by compression.

X-ray reflectivity

XRR measurements were performed at the D10AXRD2 line of Laboratório Nacional de Luz Síncrotron (LNLS, Campinas, Brazil). A monochromatic beam of 7709 eV (λ = 1.608 Å) was used to perform the experiments. Si(100) wafers were used as support substrates and were pretreated before coating. XRR experiments were performed by θ–2θ scanning in the range $\theta = 0.1°$–$2.5°$ with 0.0053° $\Delta\theta$ step. Corrections for beam decay were performed using the signal level of the beam monitor to correct the collection time. Analysis of the reflectometry curves was performed using the free software StochFit 1.7.[27] The algorithm implemented in the software divides the electron density of the thin film in small adjacent boxes and proceeds to modify the magnitude of the electron density and the roughness of the box to fit to the experimental data in a *model-free* way. Model dependent fits of the electron densities were also performed using StochFit 1.7 fitting a limited number of independent stacked layers (2 or 3) to the electron density obtained from the reflectivity data.

Electrochemical measurements

Cyclic voltammetry experiments were carried out using a potentiostat TEQ-04 equipped with a platinum mesh counter electrode and an Ag/AgCl reference electrode. Unless otherwise stated, all electrochemical experiments were performed at room temperature (*ca.* 24 °C) using a three-electrode Teflon electrochemical cell.

Atomic force microscopy

The atomic force microscopy (AFM) studies were performed using a Nanoscope IIIa-Quadrex Multimode AFM (Bruker, Santa Barbara, CA, U.S.A.) equipped with a vertical J-scanner having a maximal lateral range of approximately 150 μm. All imaging was performed in tapping-mode under dry nitrogen using silicon probes. Cantilevers for imaging in air were diving board shaped silicon microcantilevers with a nominal spring constant and a resonant frequency of 42 N m^{-1} and 300 kHz, respectively. The scan rate was 1 Hz, which allows stable AFM operation and good topographic images. Each sample was imaged several times at different locations on the substrate to ensure reproducibility. Measurements of width and height were performed using the NanoScope off-line software.

Results and discussion

Fig. 1 displays the surface pressure (π) *vs.* mean molecular area (MMA) isotherms of PBzMA-*b*-PDMAEMA diblock copolymers (2.6 kDa–1.9 kDa) obtained under different pH conditions in 0.1 M KCl. It is evident that the proton concentration in the subphase strongly influences the behavior of the block copolymer assembled at the air–water interface. PDMAEMA blocks contain tertiary amino groups displaying an average pK_a value of 7.5.[28] Rehfeldt *et al.*[29] showed that the degree of protonation of PDMAEMA at pH 5 is about 85%, at pH 7 around 23%, and at pH 8 *ca.* 13%. Hence, at pH 2 PDMAEMA blocks are fully protonated whereas at pH 10 the same monomer units are in the neutral form.

The isotherms of PBzMA-*b*-PDMAEMA spread on 0.1 M KCl at pH 10 and those performed at pH 6 and 2 are significantly different. The isotherm of PBzMA-*b*-PDMAEMA on 0.1 M KCl at pH 10 shows a sharp increase in surface pressure. Conversely, at pH 2, the surface pressure does not increase until the film was compressed to low molecular areas, indicating a major reorganization of the block copolymer at the interface upon protonation of the PDMAEMA blocks. Under these conditions the fully ionized PDMAEMA blocks are completely dissolution in the acidic aqueous subphase. Samples measured at pH 2 and 5 exhibit no measurable surface pressure for mean molecular areas above 400 $Å^2$. This fact might indicate that the crowding

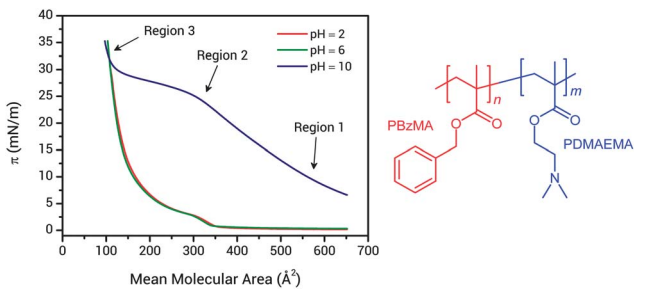

Fig. 1 π–MMA isotherms of the PBzMA-*b*-PDMAEMA diblock copolymer at pH 2, 6 and 10 and the chemical structure of the polymeric material.

caused by the self-assembly process forces the PBzMA chains into the air phase. Notably, regardless of the pH isotherms of PBzMA-*b*-PDMAEMA diblock copolymers display a well-defined transition upon compression beyond 300 Å^2.

Before going further, we first must rationalize the physicochemical processes taking place at the air–water interface.

The formation and assembly of PBzMA-*b*-PDMAEMA surface micelles relies on the delicate interplay between different factors: (a) the solubility of the protonated PDMAEMA blocks, (b) the electrostatic repulsion between the ionized PDMAEMA monomer units in the aqueous subphase, (c) the hydrophobic interactions between the PBzMA micelle cores, and (d) steric forces between neutral PDMAEMA coronas located at the air–water interface. At pH 2, in principle, the effects of the solubility and electrostatic repulsion of submerged PDMAEMA chains prevail over hydrophobic interactions in a way that the Langmuir film exhibits a low surface pressure at a large mean molecular area, thus indicating the formation of smooth and uniform monolayers.[30] Isotherms at pH 2 and 5 are rather similar and both exhibit pseudoplateaus corresponding to the so-called "*pancake-to-brush*" transition followed by a steep increase in surface pressure upon compressing the film to MMA values close to 100 Å^2.

In Region 1 (Fig. 1) the surface film expands at large molecular areas. The hydrophobic PBzMA blocks form a core above the interface to avoid unfavorable interactions with water, while PDMAEMA blocks remain anchored at the interface, forming surface micelles with a pancake-like morphology.[31]

In the "*pancake-to-brush*" transition (Region 2, Fig. 1) the PDMAEMA blocks gradually submerge in the aqueous subphase and form a conformationally extended brush-type array underneath the PBzMA segregated cores confined at the air–water interface.[32] It is evident that even if the environmental pH facilitates the dissolution of PDMAEMA blocks, chains do not spontaneously submerge into the aqueous subphase but remain at the air–water interface at low surface pressure. However, further compression leads to brush formation in which electrostatic and steric repulsion between submerged PDMAEMA chains are assumed as the main driving forces governing the π–MMA isotherms (Fig. 2). It should be noted that under highly acidic conditions PBzMA micelle cores anchored at the air–water interface could form large supramolecular aggregates due to the association of hydrophobic particles driven by hydrophobic interactions (Fig. 3).[33]

To corroborate the critical role of electrostatic interactions in determining the characteristics of the isotherm we performed similar experiments at pH 2 under different ionic strength conditions. Polyelectrolyte brushes change from an extended conformation in a solution of low ionic strength to a coiled conformation in solutions of high ionic strength.[34] Polymer chains show a strongly extended (stretched) conformation in low ionic strength solutions, as a result of both the repulsion between neighboring chains and the repulsion between the repetitive units (Fig. 4a). In contrast, when polymer brushes are placed in high ionic strength solutions, the charges of the pendant groups in the polymer chains are screened, and the

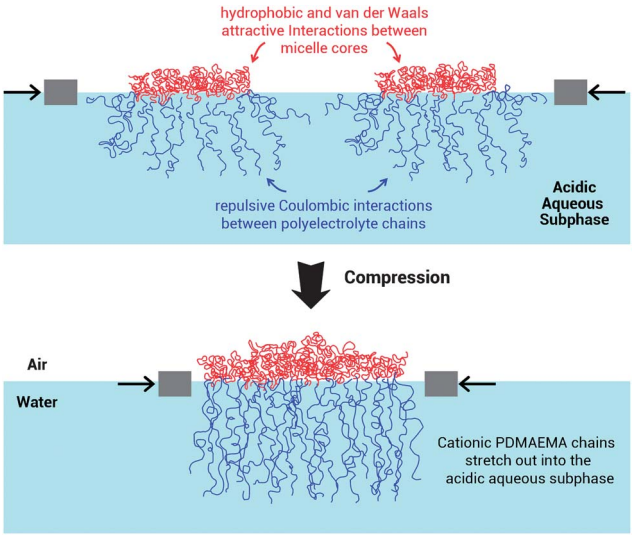

Fig. 3 Schematic illustration of the compression of the interface-confined micelles leading to the formation of stretched polyelectrolyte brushes underneath the PBzMA aggregates under acidic subphase conditions.

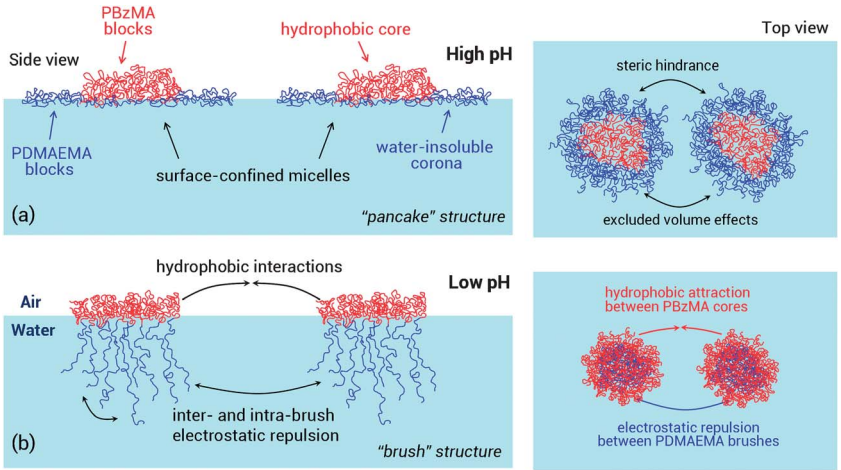

Fig. 2 Schematic illustrations (side and top views) of surface micelles formed at the air–water interface under (a) high and (b) low pH conditions.

minimization of the electrostatic repulsions leads to entropically more favorable collapsed conformations (Fig. 4a).

Fig. 4b displays the π–MMA isotherms obtained in aqueous subphases containing different concentrations of KCl. As the ionic strength of the subphase increases, the isotherms show the more condensed film behavior. It is clear that the electrostatic repulsion among the charged PDMAEMA chains is screened more effectively under higher ionic strength conditions so that the surface pressure at very high MMA sharply decreases upon increasing the concentration of KCl in the subphase. Fig. 5 shows the variation in surface pressure upon increasing the ionic strength of the subphase. Under high ionic strength conditions the plot reveals low surface pressures, which may reflect the screening of the Coulomb interactions between brush chains in the aqueous subphase.

Interestingly, mean-field models predict the scaling relationship[35] for surface pressure of annealed brushes to be:

$$\pi = N\sigma^{5/3}\left[\frac{\alpha_b^2}{\rho_s}\right]^{2/3} \quad (1)$$

where α_b is the degree of dissociation in the bulk, ρ_s is the salt concentration, N is the chain length and the grafting density σ is defined as the number of grafted chains per unit area. This implies that in the so-called "*salted brush*" regime $\pi \propto \rho_s^{-2/3}$. Despite the fact that theoretical studies predict that the annealing[36] of charge on grafted chains may result in a rather complicated physicochemical scenario due to the complex interplay between pH, salt concentration and grafting density, our experimental results reveal that a log–log plot of π *versus* electrolyte concentration has a slope of -0.68, which is very close to the theoretical value, *i.e.* -0.66.

Region 3 (Fig. 1) is the "brush" region that is governed by the interaction of the relatively incompressible PBzMA micelle cores anchored at the air–water interface and the steric and electrostatic repulsion between PDMAEMA brushes. At pH 10 the π–MMA isotherm is more expanded and interestingly the film exhibits considerably higher surface pressure at relatively high MMA values. This behavior should be mainly attributed to strong repulsive interactions, due to excluded volume effects, between interface-confined hydrophobic aggregates constituted

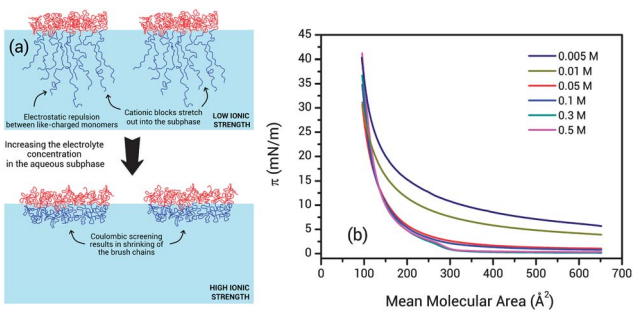

Fig. 4 (a) Schematic illustration of the conformational changes taking place in the cationic PDMAEMA brushes underneath the PBzMA aggregates upon increasing the ionic strength of the subphase. (b) π–MMA isotherms of the PBzMA-*b*-PDMAEMA diblock copolymer obtained under different subphase conditions: 0.005, 0.01, 0.05, 0.1, 0.3 and 0.5 M KCl (pH = 2).

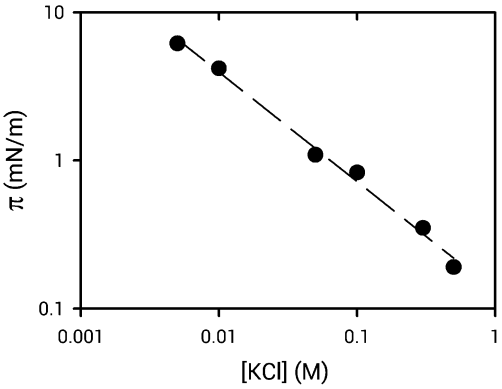

Fig. 5 Representation of surface pressure as a function of the electrolyte concentration in the acidic (pH 2) aqueous subphase. The resulting line from the linear regression analysis was also plotted (slope = −0.68).

of PMBz cores and neutral PDMAEMA shells. Conversely, in Region 3 at pH 2 the surface micelles can be compressed without a significant increase in surface pressure until micelle–micelle repulsion dominates the isotherm and consequently an abrupt surface pressure change is detected.

pH changes not only affect the isotherm behavior but the morphological aspects of the Langmuir–Blodgett films as well. Fig. 6 shows the AFM topographic images of PBzMA-*b*-PDMAEMA LB films formed on 0.1 M KCl at pH 10. The LB films were transferred at different surface pressure values in order to study the structural evolution of the transferred film. It is observed that at 15 and 20 mN m^{-1} circular micelles with a mean diameter (d) of *ca.* 9 nm coexist with isolated larger aggregates ($d \sim 60$ nm). The formation of larger aggregates could be ascribed to the spontaneous association of small block micelles[37] even at very large molecular areas. Fig. 7 depicts a comparative AFM study (topographic and phase imaging) of LB films transferred (a) in the absence of compression and (b) at 15 mN m^{-1}. AFM imaging confirms that the formation of large micellar aggregates is not triggered by the compression of the block copolymer film deposited on the aqueous surface. Indeed, AFM also reveals that in the absence of compression small surface micelles are inhomogeneously transferred to the substrate exhibiting patches of bare domains. Nevertheless, slight compression (15 mN m^{-1}) facilitates the formation of a micellar film evenly distributed on the solid substrate Fig. 6d–f. It can be clearly seen that small circular micelles form a quasi-hexagonally packed structure, which is typically observed in surface micelle morphologies of amphiphilic block copolymers with a large enough hydrophilic block.[17] For instance, the distance between the PBzMA cores reflects the hydrophilic PDMAEMA block length residing at the air–water interface as corona chains.

At $\pi = 25$ mN m^{-1} the circular micelles are in contact with each other leading to the formation of worm-like surface structures constituted of 2–3 micelles per "worm". Reduction of the intermicellar distance upon increasing π is expected; however, we observe that the interplay between the strong confinement at the air–water interface together with the

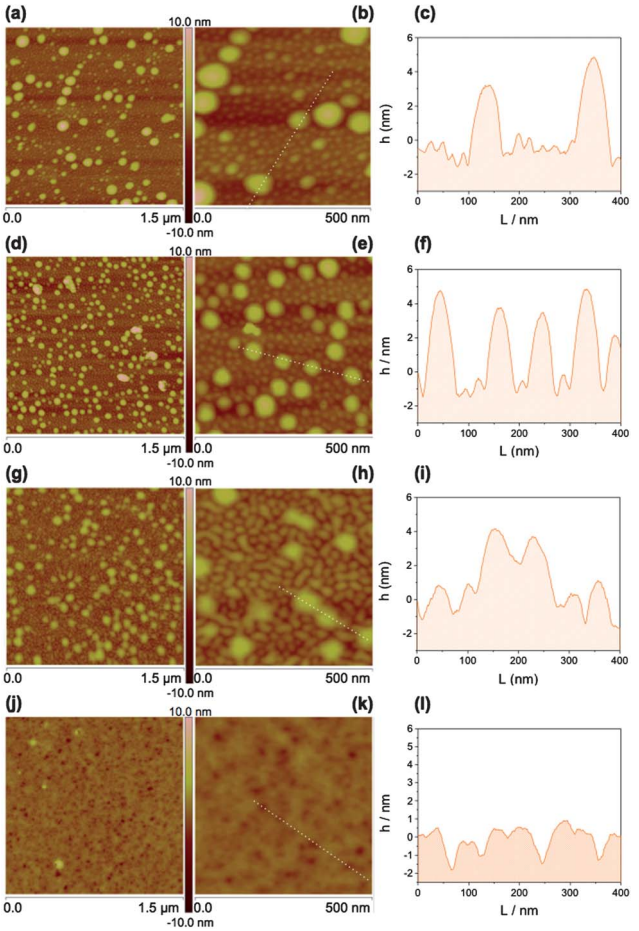

Fig. 6 Topographic AFM images at different magnifications and the corresponding cross-section analysis of PBzMA-*b*-PDMAEMA diblock copolymer LB films transferred at different surface pressures on Si: (a–c) 15 mN m^{-1}, (d–f) 20 mN m^{-1}, (g–i) 25 mN m^{-1}, and (j–l) 35 mN m^{-1}. Subphase: 0.1 M KCl (pH 10).

hydrophobic interactions between PBzMA-*b*-PDMAEMA chains triggers the association of surface micelles. This association mechanism also operates in the larger aggregates as can be seen in Fig. 6g–i.

In contrast, a significant morphological transformation comes to light at $\pi = 35$ mN m^{-1}. It is observed that further compression above the "*pancake-to-brush*" transition leads to the formation of homogeneous films. The AFM image shown in Fig. 6j–l confirmed the presence of a reasonably homogeneous PBzMA-*b*-PDMAEMA LB film. The randomly distributed holes (dark contrast in the AFM image) could possibly be formed after transfer due to some film reorganization resulting from the shrinkage/and/or dehydration of PDMAEMA during the drying step. A similar observation regarding this morphological feature has been previously reported by Joncheray *et al.*[38] referring to the two-dimensional self-assembly of polystyrene-*b*-poly(acrylic acid) dendrimer-like copolymers at the air–water interface. In order to assess the physical porosity of the block copolymer film formed, we performed cyclic voltammetry (CV) in the presence of $Fe(CN)_6^{4-/3-}$ species.[39] CV is a very effective means to detect bare/uncovered domains, *i.e.* nanopores, in the polymer film through the penetration and diffusion of redox-active probes through the film transferred onto conductive gold substrates.[40] In our case, cyclic voltammetry reveals a well-defined electrochemical response of $Fe(CN)_6^{4-/3-}$ ions which indicates that the pores connect the underlying gold substrate with aqueous solution (Fig. 8). It should be noted that blank experiments performed in the absence of a PBzMA-*b*-PDMAEMA LB film, *i.e.* bare gold substrates, displayed higher electrochemical signals. This is due to the fact that despite the porous structure, the polymer film decreases the effective surface area of the gold substrate.

AFM imaging of LB films prepared at subphase pH = 2 under different surface pressure conditions (Fig. 9) confirmed the presence of dispersed dot-like domains[41] that gradually transformed into an island-like morphology at the "*pancake-to-brush*" transition (*i.e.*, Region 2, Fig. 1). This result stands in apparent contrast to previous observations at subphase pH = 10 in which the presence of evenly distributed spherical micellar assemblies was detected. It is noteworthy that the domain height showed significant differences at different surface pressures. Indeed, AFM images reveal that the morphology transformation continues with further percolation and/or aggregation of island-like domains upon increasing compression. Nevertheless, images clearly confirm the irregular topography of the LB films prepared at high π, *i.e.* 22 mN m^{-1}. The resulting block copolymer layers exhibit an irregular continent-like morphology. Topographic imaging shows the presence of different surface domains in which the height difference is close to 4 nm. Film thicknesses obtained from X-ray reflectivity measurements are 6.3 and 6.7 nm for LB films transferred at 10 and 22 mN m^{-1}, respectively. We should consider here that as π is increased charged PDMAEMA segments are progressively compressed in the aqueous subphase forming a stretched polyelectrolyte brush underneath the PBzMA cores of the surface micelles. Concomitantly, compression of "bare" PBzMA cores at the air–water interface further promotes their aggregation into larger and thicker domains. Therefore when transferred to the solid substrate the formation of large domains of PDMAEMA brushes and PBzMA aggregates plays an important role in defining the topographic features of the obtained films.

Once again, in order to assess the physical porosity of the irregular block copolymer thin film we performed cyclic voltammetry in the presence of $Fe(CN)_6^{4-/3-}$ species. CV data show a well-defined electrochemical response of $Fe(CN)_6^{4-/3-}$ ions (Fig. 10) which indicates that the irregular film is exposing domains through which the redox probe is able to diffuse and reach the underlying conductive substrate. In fact, CV also reveals that the effective surface area of these diffusion pathways decreases after transferring the copolymer films at higher surface pressures. This functional aspect related to the structural organization of the polymeric interfacial architecture cannot be easily assessed by AFM imaging. However, the decrease of $Fe(CN)_6^{4-/3-}$ peak current densities after transferring the films at increasing π values corroborates the presence of structural transformations in the polymer films regardless of the visual aspect of their topography.

To further study the structural organization of the block copolymer film transferred onto the silicon substrate we used X-

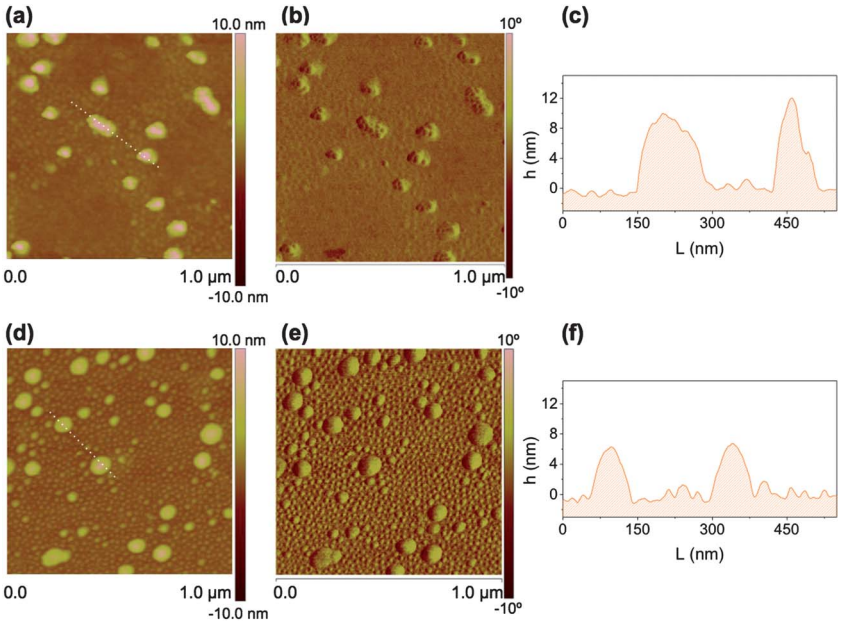

Fig. 7 Topographic and phase AFM imaging with the corresponding cross-sectional analysis of PBzMA-*b*-PDMAEMA diblock copolymer LB films transferred in (a–c) the absence of compression ($\pi = 7$ mN m^{-1}) and at (d–f) $\pi = 15$ mN m^{-1}. Subphase: 0.1 M KCl (pH 10).

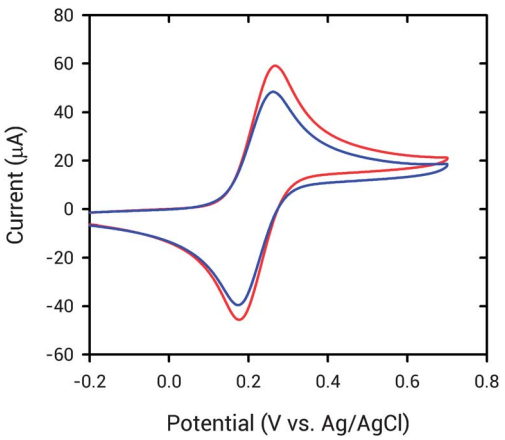

Fig. 8 Cyclic voltammograms corresponding to (red trace) a bare gold electrode (blue trace) PBzMA-*b*-PDMAEMA diblock copolymer LB film transferred at 35 mN m^{-1} on an evaporated gold, in the presence of 1 mM $Fe(CN)_6^{3-}$ + 1 mM $Fe(CN)_6^{4-}$ + 0.1 M KCl. Films were transferred using 0.1 M KCl (pH 10) as a subphase.

ray reflectivity as a powerful tool to probe the buried interfacial structure of the PBzMA-*b*-PDMAEMA diblock copolymer film. The juxtaposition of complementary structural techniques is necessary in order to elucidate the actual interfacial configuration of the transferred block copolymer films. The vast majority of reports on this subject support their conclusions by information obtained exclusively from AFM imaging. However, drawing conclusions from a "single-technique" approach can be rather speculative due to AFM is unable to provide structural information of the inner region of the transferred film. In this way we consider that the combination of AFM imaging with X-ray reflectivity may allow us to *unambiguously* correlate the interfacial structural configuration with the different surface morphologies observed in the LB films.

Considering the chemical nature of both blocks we could assume that a PBzMA layer is adjacent to the air surface and a PDMAEMA layer is adjacent to the silicon substrate. However, in previous studies it has been reported that the density profile and the structural characteristics of the interface strongly depend on the polymer–substrate interaction.[42,43] For instance, the density at the interface changes in accordance with the strength of interaction between the polymer and the substrate.[44] The graphs of reflectivity as a function of the momentum transfer vector, q_z, collected on LB films of PBzMA-*b*-PDMAEMA diblock copolymer transferred at surface pressures above the "*pancake-to-brush*" transition under alkaline and acidic aqueous subphase conditions are shown in Fig. 11a and c, respectively. These XR profiles were modeled using a nonlinear least-squares fitting using a recursive multilayer method.[27] Fig. 11b and d illustrate the scattering length density profile obtained from the model fit of the reflectivity of each LB film. It is important to note that X-ray analysis can only show the result of the electron density profile, not the material itself. The electron density of PDMAEMA is higher than that of PBzMA, especially in the case of acidic conditions in which charged PDMAEMA blocks are transferred with chloride counterions. XRR data corroborate that the organization of both blocks on the silicon substrate is strongly dependent on the pH conditions of the subphase during the LB transfer. When the PBzMA-*b*-PDMAEMA diblock copolymer films were transferred under alkaline conditions onto clean silicon wafers the best fit to the data (Fig. 11b) showed a dip in the SLD profile near the substrate which may indicate that PBzMA blocks are buried in the interfacial region and concomitantly a PDMAEMA-rich region is located in the outer region of the film.[45] A similar analysis performed on PBzMA-*b*-PDMAEMA films transferred under acidic conditions revealed the opposite scenario. Charged hydrophilic PDMAEMA

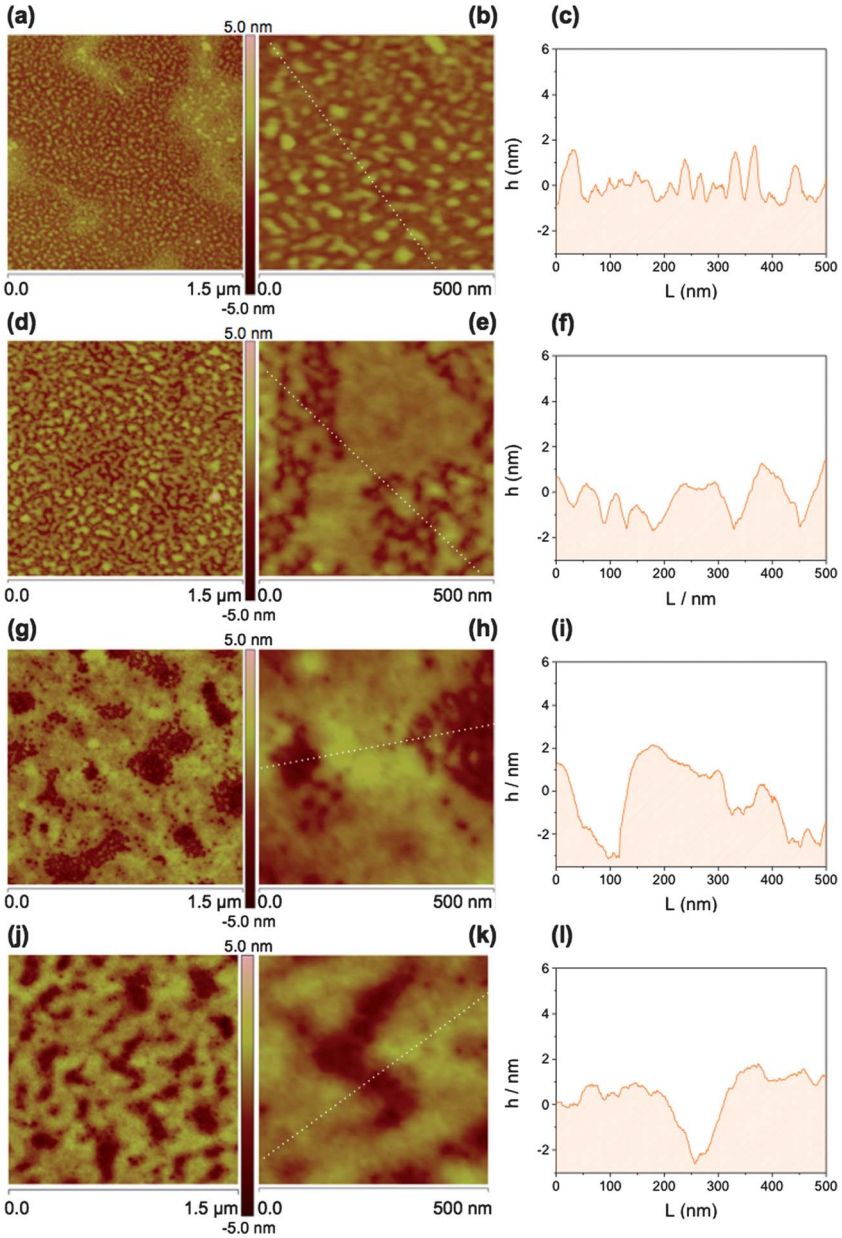

Fig. 9 Topographic AFM images at different magnifications and the corresponding cross-section analysis of PBzMA-*b*-PDMAEMA diblock copolymer LB films transferred at different surface pressures on Si: (a–c) 0.8 mN m^{-1}, (d–f) 2 mN m^{-1}, (g–i) 10 mN m^{-1}, and (j–l) 22 mN m^{-1}. Subphase: 0.1 M KCl (pH 2).

blocks are drawn back into the interface, leaving hydrophobic PBzMA segments at the surface. We believe that the driving force behind this reorganization is the strong interaction between the anionic polar native oxide on the Si substrate and the cationic PDMAEMA brushes. XRR data presented above with the corresponding two-layer model of the polymer film (Fig. 11b and d) seem to support this general picture that points to the phase segregation of the different domains occurring over length scales as large as 50 Å to 60 Å.

Compression–expansion hysteresis experiments were carried out with different target surfaces under different pH conditions (Fig. 12). At pH 2 compression–expansion experiments with target pressure 5 mN m^{-1} showed that all the compression and expansion curves overlapped, which is a good indication not only of film formation reproducibility but also thermodynamic stability (Fig. 12a). However, upon increasing the target pressure to 20 mN m^{-1} an increase in π is observed during the first barrier expansion (Fig. 12b). This observation might suggest that the disassembly kinetics of the aggregated PBzMA cores anchored at the air–water interface is slower than the barrier expansion speed. The higher π value measured after the first expansion could be ascribed to the stronger repulsion between larger domains of charged PDMAEMA blocks submerged in the acidic aqueous subphase forming an extended brush-type array underneath the aggregated PBzMA cores.

Conversely, compression–expansion hysteresis experiments carried out at target surface pressures of 25 and 35 mN m^{-1}

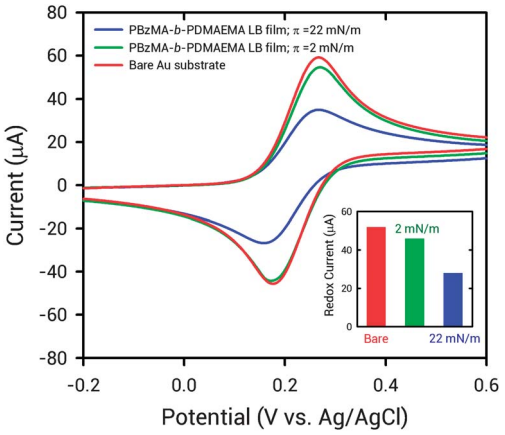

Fig. 10 Cyclic voltammograms corresponding to: (red trace) a bare gold electrode, (green trace) PBzMA-*b*-PDMAEMA diblock copolymer LB film transferred at 2 mN m^{-1} on an evaporated gold film and (blue trace) PBzMA-*b*-PDMAEMA diblock copolymer LB film transferred at 22 mN m^{-1} on an evaporated gold film, in the presence of 1 mM $Fe(CN)_6^{3-}$ + 1 mM $Fe(CN)_6^{4-}$ + 0.1 M KCl. Films were transferred using 0.1 M KCl (pH 2) as a subphase.

(Fig. 12c and d, respectively) under alkaline conditions revealed a different behavior. Regardless of the surface pressure the expansion curves exhibited a drop in pressure that corresponds to the slow reorganization of the PDMAEMA blocks forming the corona of the surface micelles. Or, in other words, PDMAEMA segments cannot return to their original conformation/configuration at low pressure after monolayer decompression.

We also studied the relaxation behavior of the block polymer films[46,47] formed at the air–water interface *via* a step compression method under different pH conditions. The basis of these experiments relies on the initial film compression and afterwards barriers are stopped to allow the relaxation of the monolayer. As shown in Fig. 13 the relaxation process is very slow and demands several minutes to reach equilibrium. We used an exponential function to fit the surface pressure curves obtained in step compression experiments.[48–50] In line with recent results by Wang *et al.*[30] we choose two exponentials to fit the relaxation curves,

$$E(t) = E_1 \exp[-t/\tau_1] + E_2 \exp[-t/\tau_2] \quad (2)$$

where E is the compression modulus, and E_1 and E_2 are the moduli corresponding to relaxation times τ_1 and τ_2, respectively. It is worth mentioning here that we corroborated that two exponential fitting curves fit the original relaxation curves better than the single exponential curve. This suggests that the relaxation process is dominated by different physical mechanisms operating with different characteristic times.

It has been recently suggested[30] that τ_1 may represent the damping dynamics of films caused by surface fluctuation from the stop of barriers whereas τ_2 reflects the arrangement of polymer aggregates inside the films which results in the conformation changes (Table 1).

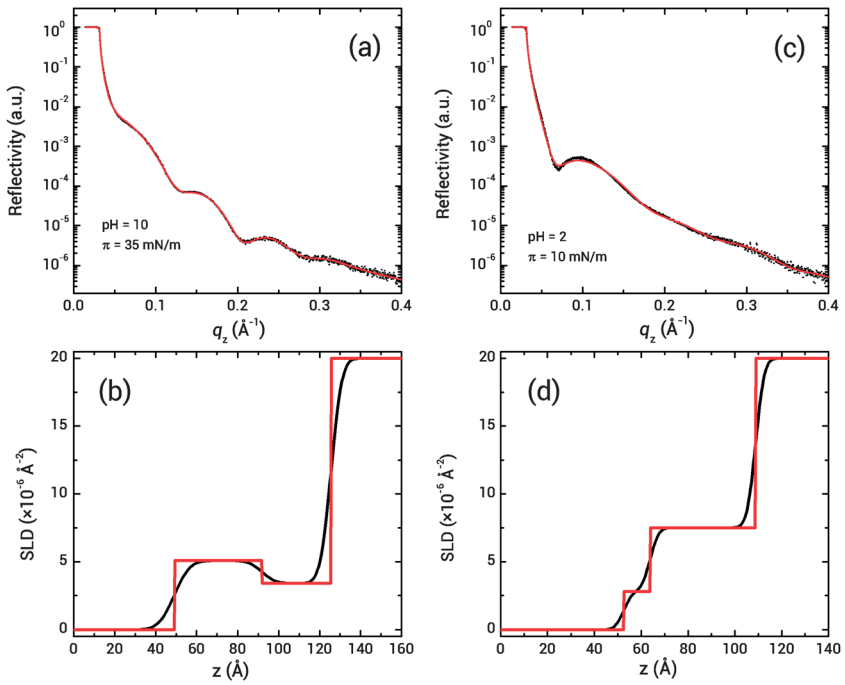

Fig. 11 (a) Specular X-ray reflectivity curve (black dots) together with a fit to the data (solid red line) from an LB film of PBzMA-*b*-PDMAEMA diblock copolymer ($\pi = 35$ mN m^{-1}, subphase: 0.1 M KCl – pH 10). Film thickness: 8.1 nm. (b) Plot of the scattering length density (SLD) as a function of the profile depth in the *z*-direction obtained from XRR data of the PBzMA-*b*-PDMAEMA diblock copolymer LB film transferred at $\pi = 35$ mN m^{-1} (subphase: 0.1 M KCl – pH 10). A two-layer slab model without roughness is depicted in red trace. (c) Specular X-ray reflectivity curve (black dots) together with a fit to the data (solid red line) from an LB film of PBzMA-*b*-PDMAEMA diblock copolymer ($\pi = 10$ mN m^{-1}, subphase: 0.1 M KCl – pH 2). Film thickness: 6.3 nm. (b) Plot of the scattering length density (SLD) as a function of the profile depth in the *z*-direction obtained from XRR data of the PBzMA-*b*-PDMAEMA diblock copolymer LB film transferred at $\pi = 10$ mN m^{-1} (subphase: 0.1 M KCl – pH 2). A two-layer slab model without roughness is depicted in red trace.

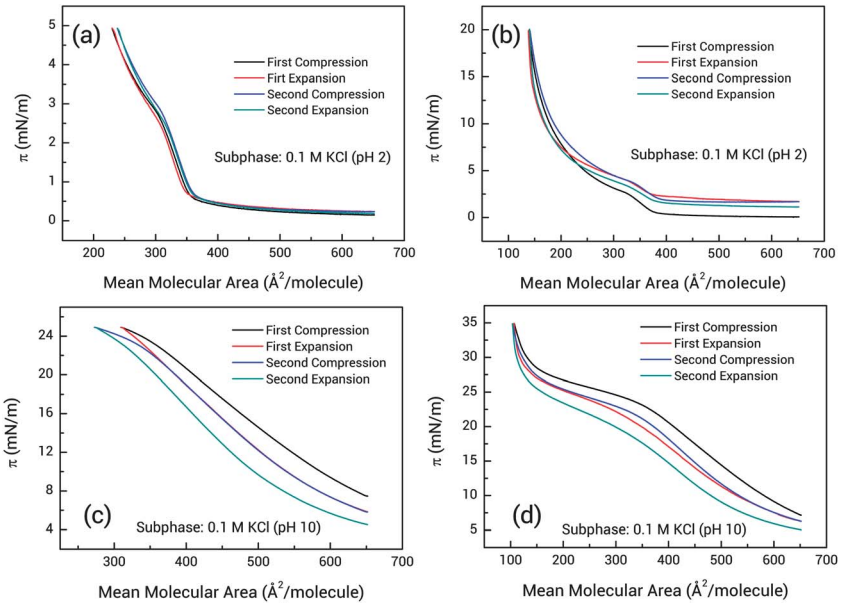

Fig. 12 Compression–expansion hysteresis plots of PBzMA-*b*-PDMAEMA diblock copolymer assemblies at the air–water interface under different conditions: (a) subphase: 0.1 M KCl (pH 2), target pressure: 5 mN m^{-1}; (b) subphase: 0.1 M KCl (pH 2), target pressure: 20 mN m^{-1}; (c) subphase: 0.1 M KCl (pH 10), target pressure: 25 mN m^{-1}; (d) subphase: 0.1 M KCl (pH 10), target pressure: 35 mN m^{-1}.

At pH 2 it is observed that the compression modulus and relaxation times increase with the decrease of the mean molecular area. This could be attributed not only to the entanglement of the core-forming PBzMA polymer chains at the air–water interface but also the entanglement of PDMAEMA brushes submerged in the acidic aqueous subphase. We should note that the relaxation of compressed surface micelles involves the diffusion of polymer chains in a dense network of entanglements formed by the surrounding chains. Hence, as we compress the monolayer, *i.e.* decreasing the MMA, we increase the topological constraints to chain motion.

Interestingly, at pH 10 relaxation times are shorter upon decreasing the mean molecular area. It is evident that different driving forces govern the relaxation process depending on the pH. PDMAEMA in its deprotonated form is surface-active, but it is still water soluble. Under alkaline conditions upon decreasing MMA, *i.e.* increasing π, PDMAEMA blocks desorb from the interface and aggregate inside the water subphase. For instance, as the films are compressed within the pseudo-plateau region, PDMAEMA chains collapse by dissolving them in the water subphase and stay in the vicinity of the interface.

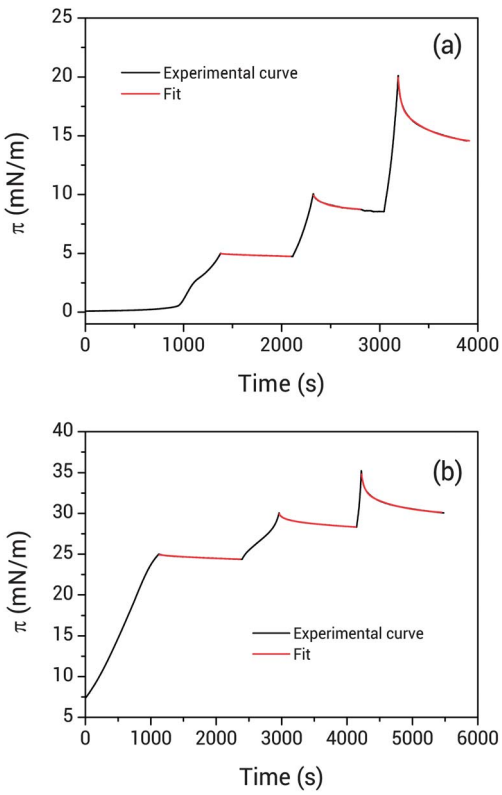

Fig. 13 Surface pressure as a function of time in two step-compression experiments (black trace) and the corresponding exponential fitting curves (red trace), at different subphase pH values. (a) pH = 2 and (b) pH = 10.

Table 1 Compression modulus and relaxation times from fits of pressure *versus* time plots according to eqn (2)

MMA (Å)	E_1 (mN m^{-1})	E_2 (mN m^{-1})	E_0 (mN m^{-1})	τ_1 (s)	τ_2 (s)
pH 2					
216	0.49	0.85	1.34	54	311
158	2.81	3.3	6.1	26	333
132	5.47	9.5	15.0	93	2275
pH 10					
292	0.007	0.89	0.90	75	1943
135	0.44	1.35	1.79	58	834
112	2.51	2.91	5.42	45	548

Regarding this latter we should mention that a similar scenario has been proposed by Joncheray and co-workers[38] for the case of polyacrylic acid (PAA) blocks in polystyrene-*b*-poly(acrylic acid) dendrimer-like copolymers spread on aqueous surfaces. In this context we hypothesize that the steric repulsion between submerged PDMAEMA chains is probably the main driving force governing the rapid relaxation kinetics of compressed micellar aggregates.

Finally we studied the influence of the spreading concentration on the physicochemical behavior aggregate morphologies of LB films. Fig. 14 displays π *vs.* MMA plots for PBzMA-*b*-PDMAEMA films prepared at a significantly higher spreading concentration (200 μl of copolymer solution 3 mg ml^{-1} in chloroform). The marked differences in isotherms obtained for a low spreading concentration point to major changes in chain conformations and packing within surface aggregates.

One of the most striking features of the isotherm is the dependence on the pH. In stark contrast to what was observed under low spreading concentration conditions, at a given MMA isotherms exhibit a pronounced increase in surface pressure upon decreasing pH.

For concentrated spreading solutions the packing of PBzMA chains within the core is relatively denser than under dilute conditions, which results in a high local density of PBzMA blocks inside the cores. The surface concentration of PBzMA blocks acting as grafting sites directly affects the nature of the interaction between PDMAEMA chains at the interface.[51] At low pH PDMAEMA segments are charged and consequently strong Coulombic repulsive interactions are expected underneath the densely packed cores. It is evident that under high spreading concentration conditions the balance between attractive hydrophobic interactions among PBzMA cores and repulsive electrostatic interactions between underwater PDMAEMA chains is significantly affected. In this case, the behaviour of the isotherm seems to be mainly governed by the electrostatic repulsion between like-charged PDMAEMA blocks.

Upon compression, submerged PDMAEMA chains are brought into contact and forced to overlap and consequently undergo a "*pancake-to-brush*" transition until the neighboring PBzMA-based surface micelle cores start to overlap. Fig. 14 eloquently illustrates the critical role of electrostatic repulsion between PDMAEMA blocks in defining the "*pancake-to-brush*" transition. It is clearly observed that an increase in pH shifts the transition toward lower MMA values. In contrast, for dilute spreading (see Fig. 1), the "*pancake-to-brush*" transition occurred at the same MMA value. AFM imaging of transferred films showed very peculiar surface morphologies rarely seen in AFM studies of linear block copolymer films prepared by the LB technique. Under acidic conditions at π = 5 mN m^{-1} films displayed the formation of large hemispherical aggregates (h = 5 nm) and continents (h = 2–3 nm) (Fig. 15a–c). We hypothesize that the formation of continents might have their origin in the coalescence and reorganization of large aggregates transferred at low surface pressures. On the other hand, these surface structures are strongly reminiscent of patterns formed from the dewetting of ultrathin films of homopolymers from solid surfaces. The dewetting mechanism for surface aggregate formation has been suggested by Cheyne and Moffitt and other authors to explain the formation of large continent structures in PS-*b*-PEO monolayers.[52–55] At π = 20 mN m^{-1} PBzMA-*b*-PDMAEMA copolymers formed well defined highly branched dendritic morphologies (Fig. 15e and f) and branched continent structures (Fig. 15d). The structural organization of the block copolymer films transferred onto silicon substrates at high spreading concentrations was characterized by X-ray reflectivity. X-ray radiation from synchrotron sources was used for the purpose of studying nanoscale structural changes in PBzMA-*b*-PDMAEMA ultrathin LB films as a function of sample preparation. It is evident at first sight that the structure of the polymer films deposited on silicon substrates is significantly altered by pH conditions of the subphase during the LB transfer process. Fig. 16a and b show the XRR data (open circles) and simulations (solid lines) of PBzMA-*b*-PDMAEMA films prepared from concentrated spreading solutions and transferred at different surface pressure values under acidic subphase conditions (pH = 2). Fitting of the XRR scans resulted in a thickness of 9.9 and 8.4 nm for films transferred at 20 and 5 mN m^{-1}, respectively. Fig. 16b illustrates the scattering length density (SLD) profile obtained from the model fit of the reflectivity data. The change in the scattering length density has been used along with the change in film thickness to elucidate structural variations in the inner environment of the polymer films. As can be seen from Fig. 16, there is a tremendous influence of the surface pressure conditions on the SLD profile.

These XR profiles were modeled using a nonlinear least-squares fitting using a multilayer method. Fig. 16c and d show the scattering length density profile obtained from the model fit of the reflectivity data. In the case of the film transferred at 5 mN m^{-1}, the electron density sharply increases in the outer region of the polymer film as well as in the interfacial region in contact with the silicon substrate (that is covered with a thin layer of native silicon oxide). This has been ascribed to the presence of PDMAEMA rich domains surrounding an intermediate "hydrophobic" zone constituted of PBzMA segments (Fig. 16c). This interpretation of the XRR data is fully in agreement with AFM images (Fig. 15a–c) that show the presence of

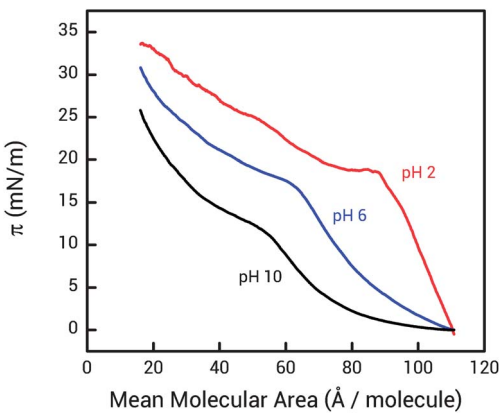

Fig. 14 π–MMA isotherms of the PBzMA-*b*-PDMAEMA diblock copolymer at pH 2, 6 and 10. Langmuir films were prepared by spreading a volume of 200 μl of 3 mg ml^{-1} copolymer solution.

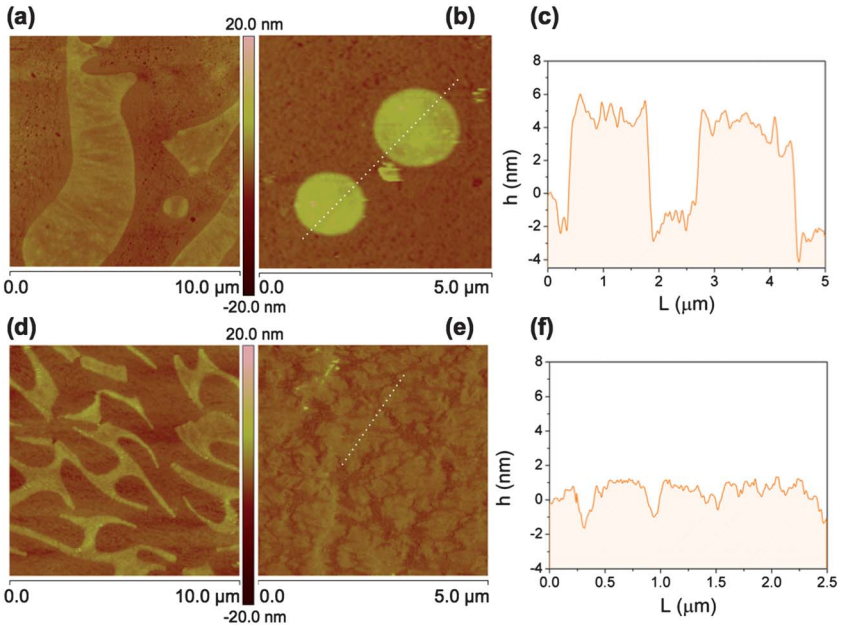

Fig. 15 Topographic AFM images at different magnifications of PBzMA-*b*-PDMAEMA diblock copolymer LB films transferred at different surface pressures on Si: (a–c) 5 mN m^{-1} and (d–f) 20 mN m^{-1}. Subphase: 0.1 M KCl (pH 2), spreading a volume of 200 μl of 3 mg ml^{-1} copolymer solution.

large micellar aggregates randomly distributed along the substrate. Indeed, the plot of the scattering length density (SLD) as a function of the profile depth in the *z*-direction indicates that these variations in SLD operate over a length scale compatible with the thickness of the micellar aggregates as determined by AFM, *i.e.* ~5 nm. It is worth mentioning that the spontaneous formation of a thin hydrophilic layer in the outer region of the polymer film is somewhat unusual since the

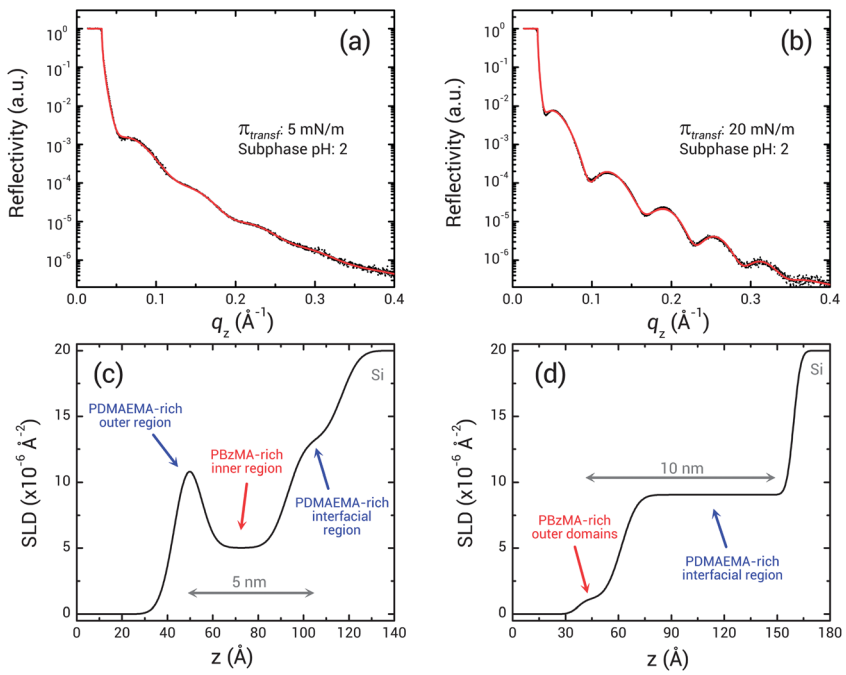

Fig. 16 (a) Specular X-ray reflectivity curve (black dots) together with a fit to the data (solid red line) from an LB film of PBzMA-*b*-PDMAEMA diblock copolymer ($\pi = 5$ mN m^{-1}, subphase: 0.1 M KCl – pH 2). Film thickness: 8.4 nm. (b) Specular X-ray reflectivity curve (black dots) together with a fit to the data (solid red line) from an LB film of PBzMA-*b*-PDMAEMA diblock copolymer ($\pi = 20$ mN m^{-1}, subphase: 0.1 M KCl – pH 2). Film thickness: 9.9 nm. (c) Plot of the scattering length density (SLD) as a function of the profile depth in the *z*-direction obtained from XRR data of the PBzMA-*b*-PDMAEMA diblock copolymer LB film transferred at $\pi = 5$ mN m^{-1} (subphase: 0.1 M KCl – pH 2). (d) Plot of the scattering length density (SLD) as a function of the profile depth in the *z*-direction obtained from XRR data of the PBzMA-*b*-PDMAEMA diblock copolymer LB film transferred at $\pi = 20$ mN m^{-1} (subphase: 0.1 M KCl – pH 2).

hydrophobic thin layer is preferred at the air interface. However, other authors have also reported this unexpected behavior in amphiphilic polymer films constituted of Nafion.[56]

Conversely, XRR characterization of LB films of PBzMA-*b*-PDMAEMA diblock copolymers transferred at 20 mN m^{-1} (Fig. 16d) indicates that the hydrophobic PBzMA blocks are located at the air–polymer interfaces whereas a more hydrophilic PDMAEMA layer is found at the silicon interface. This scenario refers to a film organization in which the lower surface tension component tends to segregate predominantly to the air interface for the lowest energy configuration. According to XRR results the SLD plot indicates that these hydrophobic PBzMA domains are occupying ~2 nm of the outermost region of the polymer film whose thickness is ~10 nm. Interestingly, AFM imaging reveals the presence of continents with thickness values close to 2 nm (Fig. 15d–f). In this context we hypothesize that the formation of branched continent structures would have their origin in the segregation of PBzMA blocks on top of uniform PDMAEMA layers.

Conclusions

In this work we investigated the surface micelle behavior of PBzMA-*b*-PDMAEMA at the air–water interface at various subphase pH and ionic strengths by surface pressure-mean molecular area isotherms and surface morphology of the LB films through a multi-technique approach. The systematic study of Langmuir isotherms combined with AFM imaging, X-ray reflectivity and electrochemical experiments of the transferred films allowed us to identify the physicochemical processes that take place at the air–water interface and correlate them with the different surface morphologies observed in the LB films. Based on these results, we could determine that at low subphase pH values the effects of the solubility and electrostatic repulsion of submerged PDMAEMA chains prevail over hydrophobic interactions and the Langmuir film exhibits low surface pressure at large molecular area values. On the other hand, under high pH subphase conditions, the isotherm is more expanded and the film exhibits higher surface pressure at relatively high MMA values due to the strong repulsive interactions between interface-confined hydrophobic aggregates constituted of PMBz cores and neutral PDMAEMA shells. In a similar way, after exploring the subphase ionic strength effect, we concluded that polymer chains show a strongly extended conformation in low ionic strength solution, as a result of both the repulsion between neighboring chains and the repulsion between the monomers, while in high ionic strength solutions, the charges of the pendant groups in the polymer chains are screened and the minimization of the electrostatic repulsions leads to entropically more favorable collapsed conformations.

Spreading copolymer solution concentration influence was also studied. The marked differences observed as concentration increases indicate critical changes in chain conformations and packing within surface aggregates. Particularly, in contrast to the results obtained under low spreading concentration conditions, π–MMA isotherms show a pronounced increase in surface pressure upon decreasing pH. Under high spreading concentration conditions, the balance between attractive hydrophobic interactions among PBzMA cores and repulsive electrostatic interactions between underwater PDMAEMA chains is significantly affected. While spreading concentration is low, the effects of the solubility of submerged PDMAEMA chains determine the film behavior, but as the concentration is increased, the isotherm seems to be governed by the electrostatic repulsion between those blocks. AFM imaging of LB films prepared under this experimental condition revealed the formation of a variety of morphologies such as highly branched dendrites, large spherical aggregates and continent-like structures.

Acknowledgements

The authors acknowledge financial support from ANPCyT (PICT Bicentenario 2010-2554, PICT-PRH 163/08, PPL 003), Centro Interdisciplinario de Nanociencia y Nanotecnología (CINN-ANPCyT-Argentina), Alexander von Humbolt Stiftung (Germany), Max-Planck-Gesellschaft (Max Planck Partner Group INIFTA/MPIP), Laboratório Nacional de Luz Síncrotron (LNLS, Brazil) (D10A-XRD2-11639, D10A – XRD2 – 14358, D10A – XRD2 – 13391) and Fundación Petruzza. M.E.C. and E.M. acknowledge CONICET for a doctoral and a postdoctoral fellowship, respectively. P.C.d.S.C., C.D., F.G.R., L.I.P., M.C and O.A. are CONICET fellows. P.C.d.S.C. gratefully acknowledges support from Universidad Nacional de La Plata (*Subsidio para viajes y estadías 2012*).

References

1 M. Lazzari and C. De Rosa, in *Block Copolymers in Nanoscience*, ed. M. Lazzari, *et al.*, VCH-Wiley, Weinheim, 2006, ch. 9, pp. 191–231.
2 M. Geoghegan and R. A. L. Jones, in *Block Copolymers in Nanoscience*, ed. M. Lazzari, *et al.*, VCH-Wiley, Weinheim, 2006, ch. 12, pp. 275–290.
3 M. Aizawa and J. M. Buriak, *Chem. Mater.*, 2007, **19**, 5090–5101.
4 Y. Park, Y.-W. Choi, S. Park, C. S. Cho, M. J. Fasolka and D. Sohn, *J. Colloid Interface Sci.*, 2005, **283**, 322–328.
5 S. Harirchian-Saei, M. C. P. Wang, B. G. Gates and M. G. Moffitt, *Langmuir*, 2010, **26**, 5998–6008.
6 K. L. Genson, J. Holzmueller, C. Jiang, J. Xu, J. D. Gibson, E. R. Zubarev and V. V. Tsukruk, *Langmuir*, 2006, **22**, 7011–7015.
7 D. T. Balogh, M. Ferreira and O. N. Oliveria, in *Functional Polymer Films*, ed. R. C. Advincula and W. Knoll, VCH-Wiley, Weinheim, 2011, vol. 1, ch. 4, pp. 113–149.
8 J. H. Park and R. C. Advincula, *Soft Matter*, 2011, **7**, 9829–9843.
9 D. H. McCullough and S. L. Regen, *Chem. Commun.*, 2004, 2787–2791.
10 S. Nagano, Y. Matsushita, S. Shinma, T. Ishizone and T. Seki, *Thin Solid Films*, 2009, **518**, 724–728.
11 E. W. Price, Y. Guo, C.-W. Wang and M. G. Moffitt, *Langmuir*, 2009, **25**, 6398–6406.

12 J. Kumaki and T. Hashimoto, *J. Am. Chem. Soc.*, 1998, **120**, 423–424.
13 T. S. Joncheray, K. M. Denoncourt, C. Mathieu, M. A. R. Meier, U. S. Schubert and R. S. Duran, *Langmuir*, 2006, **22**, 9264–9271.
14 Y. Kim, J. Pyun, J. M. J. Fréchet, C. J. Hawker and C. W. Frank, *Langmuir*, 2005, **21**, 10444–10458.
15 I. I. Perepichka, A. Badia and C. G. Bazuin, *ACS Nano*, 2010, **4**, 6825–6835.
16 K. Kita-Tokarczyk, M. Junginger, S. Belegrinou and A. Taubert, *Adv. Polym. Sci.*, 2011, **242**, 151–201.
17 B. Chung, M. Choi, M. Ree, J. C. Jung, W. C. Zin and T. Chang, *Macromolecules*, 2006, **39**, 684–689.
18 J. N. Baskir, T. A. Hatton and U. W. Suter, *Macromolecules*, 1987, **20**, 1300–1311.
19 M. Niwa, T. Hayashi and N. Higashi, *Langmuir*, 1990, **6**, 263–268.
20 E. P. K. Currie, A. B. Sieval, M. Avena, H. Zuilhof, E. J. R. Sudhölter and M. A. Cohen Stuart, *Langmuir*, 1999, **15**, 7116–7118.
21 P. Muller, G. Sudre and O. Théodoly, *Langmuir*, 2008, **24**, 9541–9550.
22 M. Niwa, N. Katsurada and N. Higashi, *Macromolecules*, 1988, **21**, 1878–1880.
23 I. B. Dicker, G. M. Cohen, W. B. Farnham, W. R. Hertler, E. D. Laganis and D. Y. Sogah, *Macromolecules*, 1990, **23**, 4034–4041.
24 O. W. Webster, *J. Polym. Sci., Part A: Polym. Chem.*, 2000, **38**, 2855–2860.
25 O. W. Webster, *Adv. Polym. Sci.*, 2004, **167**, 1–34.
26 V. Bütün, M. Vamvakaki, N. C. Billingham and S. P. Armes, *Polymer*, 2000, **41**, 3173–3182.
27 S. M. Danauskas, D. Li, M. Meron, B. Lin and K. Y. C. Lee, *J. Appl. Crystallogr.*, 2008, **41**, 1187–1193.
28 P. van de Wetering, N. J. Zuidam, M. J. van Steenbergen, O. A. G. J. van der Houwen, W. J. Underberg and W. E. Hennink, *Macromolecules*, 1998, **31**, 8063–8068.
29 F. Rehfeldt, R. Steitz, S. P. Armes, R. von Klitzing, A. P. Gast and M. Tanaka, *J. Phys. Chem. B*, 2006, **110**, 9171–9176.
30 X. Wang, X. Ma and D. Zang, *Soft Matter*, 2013, **9**, 443–453.
31 J. Zhu, A. Eisenberg and R. B. Lennox, *Macromolecules*, 1992, **25**, 6541–6555.
32 P. Kaewsaiha, K. Matsumoto and H. Matsuoka, *Langmuir*, 2004, **20**, 6754–6761.
33 S. Nagano, Y. Matsushita, Y. Ohnuma, S. Shinma and T. Seki, *Langmuir*, 2006, **22**, 5233–5236.
34 P. Kaewsaiha, K. Matsumoto and H. Matsuoka, *Langmuir*, 2007, **23**, 7065–7071.
35 E. P. K. Currie, A. B. Sieval, G. J. Fleer and M. A. Cohen Stuart, *Langmuir*, 2000, **16**, 8324–8333.
36 A distinction is generally made between brushes consisting of grafted polyelectrolytes with a fixed fraction of charged monomers (*quenched*) and polyelectrolytes with a variable fraction of charged monomers (*annealed*). In the latter case, the charge density not only depends on the pH and the salt concentration, but also on the grafting density.
37 A. Blanazs, S. P. Armes and A. J. Ryan, *Macromol. Rapid Commun.*, 2009, **30**, 267–277.
38 T. J. Joncheray, S. A. Bernard, R. Matmour, B. Lepoittevin, R. J. El-Khouri, D. Taton, Y. Gnanou and R. S. Duran, *Langmuir*, 2007, **23**, 2531–2538.
39 Y. Li, H. C. Maire and T. Ito, *Langmuir*, 2007, **23**, 12771–12776.
40 H. C. Maire, S. Ibrahim, Y. Li and T. Ito, *Polymer*, 2009, **50**, 2273–2280.
41 L. Zhao, M. Byun, J. Rzayev and Z. Lin, *Macromolecules*, 2009, **42**, 9027–9033.
42 A. van der Lee, L. Hamon, Y. Holl and Y. Grohens, *Langmuir*, 2001, **17**, 7664–7669.
43 E. K. Lin, W.-l. Wu and S. K. Satija, *Macromolecules*, 1997, **30**, 7224–7231.
44 C. Bollinne, V. W. Stone, V. Carlier and A. M. Jonas, *Macromolecules*, 1999, **32**, 4719–4724.
45 S. Ahn, J.-H. Kim, J. H. Kim, J. C. Jung, T. Chang, M. Ree and W.-C. Zin, *Langmuir*, 2009, **25**, 5667–5673.
46 F. Monroy, L. R. Arriaga and D. Langevin, *Phys. Chem. Chem. Phys.*, 2012, **14**, 14450–14459.
47 H. M. Hilles, F. Ortega, R. G. Rubio and F. Monroy, *Phys. Rev. Lett.*, 2004, **92**, 255503.
48 F. Monroy, H. M. Hilles, F. Ortega and R. G. Rubio, *Phys. Rev. Lett.*, 2003, **91**, 268302.
49 T. Scopigno, R. Di Leonardo, G. Ruocco, A. Q. R. Baron, S. Tsutsui, F. Bossard and S. N. Yannopoulos, *Phys. Rev. Lett.*, 2004, **92**, 025503.
50 H. Hilles, A. Maestro, F. Monroy, F. Ortega, R. G. Rubio and M. G. Velarde, *J. Chem. Phys.*, 2007, **126**, 124904.
51 R. B. Cheyne and M. G. Moffitt, *Langmuir*, 2005, **21**, 5453–5460.
52 R. B. Cheyne and M. G. Moffitt, *Langmuir*, 2006, **22**, 8387–8396.
53 J. K. Cox, K. Yu, B. Constantine, A. Eisenberg and R. B. Lennox, *Langmuir*, 1999, **15**, 7714–7718.
54 C. A. Devereaux and S. M. Baker, *Macromolecules*, 2002, **35**, 1921–1927.
55 Q. Lu and C. G. Bazuin, *Nano Lett.*, 2005, **5**, 1309–1314.
56 S. Kim, K. A. Page and C. L. Soles, in *Polymers for energy storage and delivery: Polyelectrolytes for batteries and fuel cells*, ed. K. Page, *et al.*, ACS Symposium Series 1096, American Chemical Society, Washington, DC, 2012, ch. 16, pp. 267–281.

